Indian J. Phys. **71B** (3), 263–280 (1997)

IJP B
— an international journal

Correlation Effects in Low-Energy Photoexcitation, Photoionization and Scattering

W. R. Johnson
Department of Physics, University of Notre Dame
Notre Dame, IN 46556, USA

Abstract: The role of electron correlation in low-energy photoexcitation, photoionization, and elastic electron-atom scattering is reviewed. Second-order core-shielding corrections and higher-order RPA corrections are considered. The quasiparticle equation and Brueckner orbitals are introduced to treat third-order core-polarization corrections. Applications are given to the photoexcitation and photoionization of cesium and to elastic electron-xenon scattering.

Keywords: electron correlation, photoexcitation, photoionization, electron-atom scattering, core shielding, core polarization

PACS numbers: 32.80.Fb, 34.80.Bm, 32.70.Cs

1. Introduction

The central-field approximation gives a simple and qualitatively correct description of atomic transition processes, such as photoionization or elastic scattering. For low energies, however, the central-field is often quantitatively incorrect. The inadequacy of the central-field approximation has two sources, core shielding and core polarization.

By *core shielding*, we are referring to the fact that an external field applied to an atom induces a secondary field in the atomic core, which, at least

in the case of an applied dipole field, reduces the size of the original field. A valence or scattering electron in the atom responds to the sum of the applied and induced fields; *i.e.*, to the shielded field. The shielding correction arises in a natural way in many-body perturbation theory (MBPT) as the second-order correlation correction to transition amplitudes. [1]

Core polarization describes the reaction of an outer (valence or scattering) electron to the multipole moments that it induces in the atomic core. Such an electron interacts with the atomic core through the sum of the original core potential and the induced multipole potential. The induced potential is attractive so the valence electron becomes more tightly bound than an electron moving in the unperturbed core potential.

In some respects, the best choice of a central potential for studies of atomic transitions or electron scattering is the Hartree-Fock (HF) potential.* One important reason for this choice is that first-order corrections to binding energies in the HF potential vanish. Since scattering phase shifts are related to valence-electron binding energies through quantum defect theory, it follows that there are no first-order corrections to scattering phase shifts calculated in a HF potential.

Starting from the HF potential, one infers from the above discussion that an outer electron in an atom moves in a potential that is the sum of the HF potential and the polarization potential. The correction to the one-electron HF energies due to the polarization potential is obtained in a straight-forward way using second-order MBPT. The core-polarization correction to the energy is the expectation value of a non-local operator, often referred to as the self-energy operator.[3] The modified HF equation arising when one adds the self-energy operator to the HF potential is referred to as the *quasiparticle* equation.[4] The corresponding single-particle wave functions are referred to as quasiparticle orbitals or as *Brueckner orbitals*.[2]

Replacing HF orbitals by Brueckner orbitals usually reduces the magnitude of transition amplitudes since the Brueckner orbitals have shorter range than the HF orbitals. In a systematic treatment of perturbation theory starting from the HF central-field approximation, the first-order transition amplitudes are those evaluated using the unperturbed HF orbitals. The second-order amplitudes give the leading core-shielding corrections. The third-order transition amplitudes consist of four distinct parts: third-order core-shielding corrections, third-order core-polarization corrections, third-order structural radiation [5] corrections, and third-order normalization corrections. The dom-

*For heavy atoms, where relativistic corrections are significant, we replace the HF potential by its relativistic counterpart, the Dirac-Hartree-Fock (DHF) potential.

inant third-order corrections are those from core polarization. These third-order core-polarization corrections are most easily obtained by solving the quasiparticle equation and then evaluating the transition matrix element using the resulting Brueckner orbitals.

2. Hartree-Fock Transition Amplitudes

As a preliminary to our discussion of correlation corrections, let us examine photoexcitation and photoionization in atomic cesium in the HF approximation. In its ground state, cesium consists of a single valence electron moving in the self-consistent field of a closed xenon-like core. As a first step in analyzing transitions in cesium, one solves the coupled Dirac-Hartree-Fock (DHF) equations:

$$(h_0 + V_{\mathrm{HF}})\, u_a = \varepsilon_a u_a$$

for the occupied core orbitals u_a and the self-consistent potential V_{HF}. In the relativistic case, there are 17 distinct orbitals corresponding to the subshells

$$(1s)^2\,(2s)^2\,(2p)^6\,(3s)^2\,(3p)^6\,(3d)^{10}\,(4s)^2\,(4p)^6\,(4d)^{10}\,(5s)^2\,(5p)^6$$

of the closed-shell Cs^+ ion. Keep in mind that the $(np)^6$ subshells separate into $(np_{1/2})^2$ and $(np_{3/2})^4$ fine-structure components and that the $(nd)^{10}$ subshells separate into $(nd_{3/2})^4$ and $(nd_{5/2})^6$ components.

Once the self-consistent potential has been determined, one solves the DHF equations for the valence electron in the *frozen* ionic core. In Table 1, we compare the DHF energies of a few low-lying states of cesium with measured energies [6]. We see from this comparison that the DHF theory for cesium predicts energies accurate to about 10%. The counterpart of energies for continuum states are scattering phase shifts. A continuum electron in the field of the Cs^+ ion experiences the long-range ionic Coulomb field together with a short-range DHF field. The phase shift, correspondingly, can be divided into the sum of an ionic Coulomb-field phase shift and a short-range phase shift. In Fig. 1, we show the short-range phase shifts for p-wave scattering from Cs^+ at low energies obtained by solving the continuum DHF equations. The zero-energy phase shifts can be inferred from energies of highly-excited states using *quantum-defect* theory [7]. As can be seen from the figure, DHF calculations give short-range phase shifts that agree at threshold with the experimental predictions at the 10% level of accuracy.

Electric dipole transition amplitudes (reduced matrix elements of the

Table 1. Comparison of DHF binding energies in cesium with the experimental energies inferred from Moore's tables [6].

State	DHF	Experiment
$6s_{1/2}$	-0.12737	-0.14310
$6p_{1/2}$	-0.08562	-0.09217
$6p_{3/2}$	-0.08379	-0.08964
$7s_{1/2}$	-0.05519	-0.05865
$7p_{1/2}$	-0.04202	-0.04393
$7p_{3/2}$	-0.04137	-0.04310
$6d_{3/2}$	-0.03609	-0.04018
$6d_{5/2}$	-0.03609	-0.03998
$8s_{1/2}$	-0.03095	-0.03230

electric dipole operator z) for alkali-metal atoms are easily evaluated in the HF approximation. For heavy alkalis, such as cesium, these amplitudes are in relatively poor agreement with precisely measured values. As an example, the following values are obtained for the amplitudes of the principal transitions in cesium from DHF calculations and from precise measurements [8], respec-

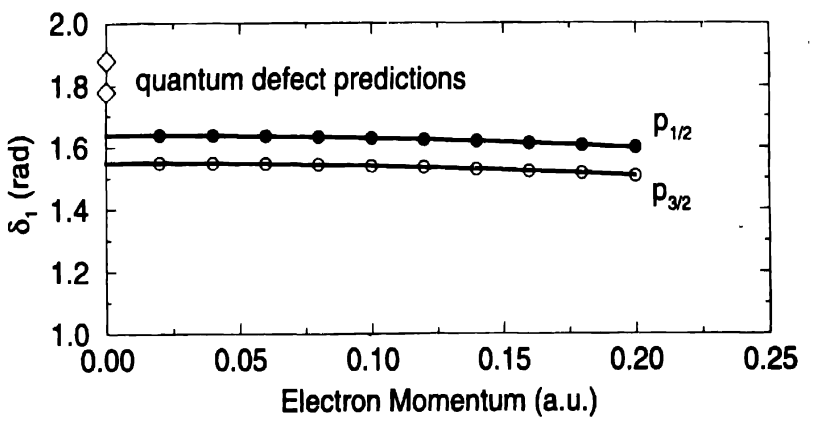

Fig. 1. Electron-Cs^+ p-wave scattering phase shifts at small values of electron momentum. The symbol ◊ represents phase shifts inferred from experiment using quantum defect theory.

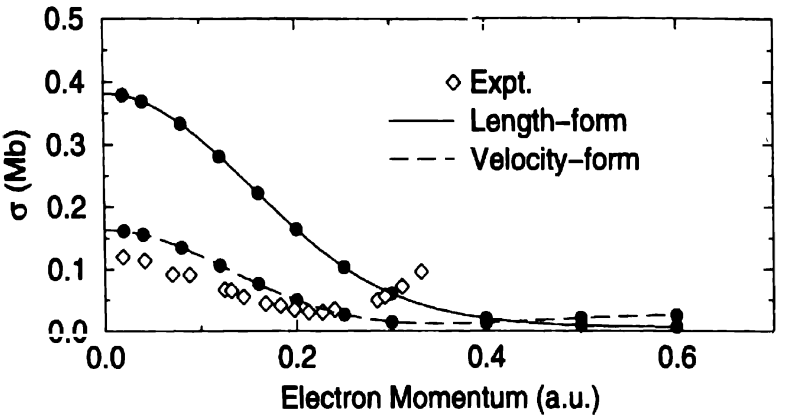

Fig. 2. DHF calculations of the cesium photoionization cross section. Both length- and velocity-form results are presented. ◊ represents experimental measurements [9].

tively:

Transition	DHF	Experiment
$6s \rightarrow 6p_{1/2}$	5.278	4.499(6)
$6s \rightarrow 6p_{3/2}$	7.426	6.332(7)

Since transition rates are proportional to the squares of the amplitudes, the 15% errors in the DHF amplitudes seen above reflect in 30% errors in the corresponding decay rates.

As a second example, we show in Fig. 2 the results of a DHF calculation of the cesium photoionization cross section at low energies, together with the experimentally measured cross section [9]. Two features are immediately apparent from this figure: first, the DHF predictions are quite different when the velocity form of the dipole operator is used instead of the length form; and second, the minimum in the experimental cross near $p = 0.2$ a.u. is not evident in the DHF cross sections.

To summarize, the DHF predictions of transition amplitudes to excited or continuum states are only qualitatively correct. To obtain quantitative predictions, one must consider correlation corrections.

3. Core Shielding and RPA

If we let $|v\rangle$ and $|w\rangle$ represent DHF orbitals for valence states v and w,

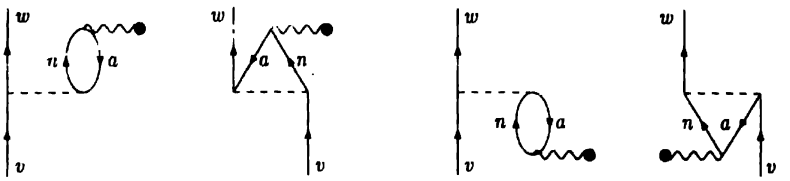

Fig. 3. Diagrams for second-order corrections to transition matrix elements.

respectively, then, in lowest-order perturbation theory, the expression for the $v \to w$ dipole transition matrix element is

$$Z^{(1)}_{wv} = z_{wv} = \langle w|z|v\rangle .$$

The corresponding reduced matrix element is precisely the DHF transition amplitude discussed in the previous section. Second-order perturbation theory leads to the correction [10]:

$$Z^{(2)}_{wv} = \sum_{an} \frac{z_{an}\tilde{v}_{wnvn}}{\varepsilon_a - \varepsilon_n - \omega} + \sum_{an} \frac{\tilde{v}_{wavn}z_{na}}{\varepsilon_a - \varepsilon_n + \omega} . \tag{1}$$

Here, ε_a and ε_n are energies of occupied and virtual levels, respectively, and $\omega = \varepsilon_w - \varepsilon_v$ is the transition energy. The notation used here and in the sequel is as follows: letters at the beginning of the alphabet a, b, ... represent occupied core states; letters near the center m, n, ... represent virtual states, and letters at the end v, w, ... represent valence states. We use i, j, ... to represent both core and virtual states. The quantities v_{ijkl} are two-particle matrix elements of the Coulomb interaction,

$$v_{ijkl} = \langle\, ij \,|\frac{1}{r_{12}}|\, kl \,\rangle ,$$

and the quantity $\tilde{v}_{ijkl} = v_{ijkl} - v_{ijlk}$ is an antisymmetrized Coulomb matrix element. The second-order corrections are represented graphically by the Brueckner-Goldstone diagrams of Fig. 3. The rules for constructing these diagrams are given, for example, in Ref. [1].

The second-order corrections for the principal transitions in cesium reduce the discrepancies with experiment discussed in the previous section

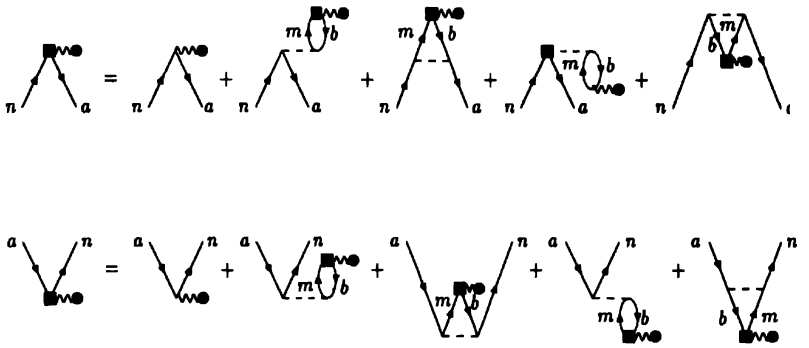

Fig. 4. Diagrams representing the RPA equations Eq.(2).

somewhat. Indeed, we find,

Transition	$Z^{(1)}$	$Z^{(2)}$	Sum	Experiment
$6s \rightarrow 6p_{1/2}$	5.278	-0.334	4.943	4.499(6)
$6s \rightarrow 6p_{1/2}$	7.426	-0.453	6.973	6.332(7)

The transition matrix elements z_{an} and z_{na} appearing in the numerator of Eq. (1) are also subject to shielding corrections. The second-order corrections to these matrix elements is given by the second-term in the iteration solution to the random-phase approximation (RPA) equations:

$$Z^{\mathrm{RPA}}_{an} = z_{an} + \sum_{bm} \frac{Z^{\mathrm{RPA}}_{bm}\,\tilde{v}_{amnb}}{\varepsilon_b - \varepsilon_m - \omega} + \sum_{bm} \frac{\tilde{v}_{abnm} Z^{\mathrm{RPA}}_{mb}}{\varepsilon_b - \varepsilon_m + \omega}$$

$$Z^{\mathrm{RPA}}_{na} = z_{na} + \sum_{bm} \frac{Z^{\mathrm{RPA}}_{bm}\,\tilde{v}_{nmab}}{\varepsilon_b - \varepsilon_m - \omega} + \sum_{bm} \frac{\tilde{v}_{nbam} Z^{\mathrm{RPA}}_{mb}}{\varepsilon_b - \varepsilon_m + \omega} \qquad (2)$$

The Brueckner-Goldstone diagrams representing the RPA equations are shown in Fig. 4. In this figure, the grey boxes are used to represent *dressed* matrix elements Z^{RPA}_{an} or Z^{RPA}_{na}. The RPA equations are widely used in atomic, nuclear, and plasma physics to describe core-shielding corrections to transition matrix elements. They may be recast in terms of coupled differential equations, the linearized time-dependent Hartree Fock (TDHF) equations,

Table 2. Iteration solution to the RPA equations for the $6p_{1/2} \rightarrow 7s$ transition in cesium.

n	δZ	Z	δV	V
		5.278		5.037
1	-0.334	4.943	-0.056	4.981
2	0.076	5.019	0.028	5.009
3	-0.067	4.952	-0.036	4.973
4	0.040	4.992	0.013	4.986
5	-0.028	4.964	-0.014	4.972
6	0.019	4.982	0.007	4.979
7	-0.012	4.969	-0.006	4.973
8	0.009	4.978	0.004	4.976
9	-0.006	4.972	-0.003	4.974
10	0.004	4.976	0.002	4.975
11	-0.003	4.974	-0.001	4.974
12	0.002	4.975	0.001	4.975
13	-0.001	4.974	-0.001	4.974
14	0.001	4.975	0.000	4.975

or solved iteratively, starting with the approximation $Z_{an}^{\mathrm{RPA}} \approx z_{an}$ and $Z_{na}^{\mathrm{RPA}} \approx z_{na}$. If we iterate the RPA equations once to obtain the second-order core-shielding corrections to z_{an} and z_{na}, and use the resulting values in Eq. (1), we obtain the third-order core-shielding corrections to z_{wv} mentioned in the introduction. If we carry through the complete iteration solution to Eq. (2) and use the results in Eq. (1), we obtain amplitudes corrected to all-orders in perturbation theory for core shielding.

The all-order RPA amplitudes are gauge-independent. As a consequence, differences between length- and velocity-form amplitudes, that lead to ambiguities in the HF case, disappear when RPA amplitudes are used. In Table 2, we show how the length- and velocity-form amplitudes (Z and V) for the $6p_{1/2} \rightarrow 7s$ transition in cesium converge order-by-order to values that are identical in length and velocity forms as we iterate the RPA equations. The convergence of perturbation theory is seen to be extremely slow for cesium. However, by 14th order we obtain amplitudes that agree in length and veloc-

ity forms to 4 significant figures. Moreover, we find that the third- and higher-order core-shielding corrections give the value 4.975 for the $6p_{1/2} \rightarrow 7s$ amplitude, quite close to second-order value 4.943, but gauge independent! Comparing with the accurately measured value 4.499(6), it is apparent that core-shielding corrections alone are not adequate for a quantitative understanding of the amplitudes. It is a straight-forward exercise to determine the RPA modifications of the photoionization cross section for cesium shown in Fig. 2; the RPA cross section lies between the DHF length-form and velocity-form curves in the figure. As for discrete transitions, the RPA cross section is gauge invariant, but accounts only qualitatively for the observed cross section. To obtain quantitatively accurate predictions, one must go beyond the RPA and consider core-polarization corrections.

4. Core Polarization and Brueckner Orbitals

In the previous section, we considered the third- and higher-order core-shielding (RPA) corrections to transition amplitudes; but, as mentioned in the introduction, there are three other third-order corrections: the core-polarization or Brueckner-orbital (BO) corrections, the structural radiation (SR) corrections, and the normalization corrections (Norm).

The dominant third-order corrections are the BO corrections, given by the equation [10]:

$$
\begin{aligned}
Z_{wv}^{\mathrm{BO}} = &- \sum_{abm\, i \neq v} \frac{z_{wi} v_{imab} v_{abvm}}{(\varepsilon_i - \varepsilon_v)\,(\varepsilon_v + \varepsilon_m - \varepsilon_a - \varepsilon_b)} \\
&+ \sum_{amn\, i \neq v} \frac{z_{wi} v_{ianm} \tilde{v}_{nmva}}{(\varepsilon_i - \varepsilon_v)\,(\varepsilon_m + \varepsilon_n - \varepsilon_a - \varepsilon_v)} \\
&- \sum_{abm\, i \neq w} \frac{\tilde{v}_{wmab} v_{abim} z_{iv}}{(\varepsilon_w + \varepsilon_m - \varepsilon_a - \varepsilon_b)\,(\varepsilon_i - \varepsilon_w)} \\
&- \sum_{amn\, i \neq w} \frac{v_{wanm} v_{nmia} z_{iv}}{(\varepsilon_m + \varepsilon_n - \varepsilon_a - \varepsilon_w)\,(\varepsilon_i - \varepsilon_w)}
\end{aligned}
\tag{3}
$$

Diagrams for the four "direct" contributions in Eq. (3), obtained by replacing $\tilde{v}_{ijkl}$ by v_{ijkl}, are shown in Fig. 5.

This equation can be written in a more compact form in terms of the self-energy operator $\sum(\varepsilon)$ mentioned in the introduction. This is the opera-

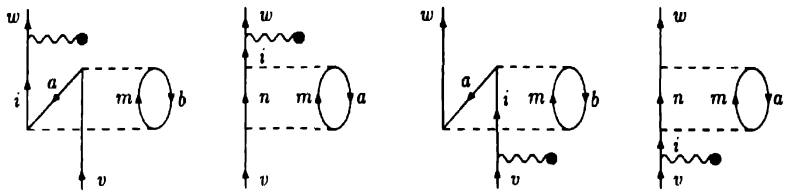

Fig. 5. Four of the eight third-order Brueckner-orbital corrections to transition amplitudes.

tor that accounts for the interaction of a valence electron, having energy ε, with the moments it induces in the core. The self-energy operator has a perturbation expansion

$$\sum(\varepsilon) = \sum^{(2)}(\varepsilon) + \sum^{(3)}(\varepsilon) + \ldots .$$

Matrix elements of the leading term in this expansion are

$$\sum_{ij}^{(2)}(\varepsilon) = \sum_{abm} \frac{v_{imab}\tilde{v}_{abjm}}{\varepsilon + \varepsilon_m - \varepsilon_a - \varepsilon_b} - \sum_{amn} \frac{v_{ianm}\tilde{v}_{nmja}}{\varepsilon_m + \varepsilon_n - \varepsilon_a - \varepsilon} .$$

Asymptotically, the self-energy operator reduces to the local dipole potential

$$\sum(r', r, \varepsilon) \to \frac{\alpha_d}{2r^2}\delta(r' - r) .$$

The wave function φ for a valence electron interacting with the moments it induces in the core satisfies the quasiparticle equation [4]:

$$[h_0 + V_{\mathrm{HF}} + \Sigma(\varepsilon)]\,\varphi = \varepsilon\varphi \qquad (4)$$

As mentioned earlier, this wave function φ is referred to as the quasiparticle orbital or Brueckner orbital. If we expand the Brueckner orbital in a perturbation series, starting with the HF orbital u_v, and expand the quasiparticle energy ε in a series starting with the HF energy ε_v,

$$\varphi = u_v + \varphi_v^{(2)} + \ldots + \varepsilon = \varepsilon_v + \varepsilon_v^{(2)} + \ldots , \qquad (5)$$

Table 3. Theoretical energies for cesium, including second-order correlation corrections, are compared with experimental energies [6].

State	DHF	$\varepsilon^{(2)}$	Sum	Experiment
$6s_{1/2}$	-0.12737	-0.01774	-0.14511	-0.14310
$6p_{1/2}$	-0.08562	-0.00691	-0.09253	-0.09217
$6p_{3/2}$	-0.08379	-0.00618	-0.08997	-0.08964
$7s_{1/2}$	-0.05519	-0.00420	-0.05939	-0.05865

then the second-order correction to φ satisfies the inhomogeneous equation:

$$[h_0 + V_{\mathrm{HF}} - \varepsilon_v]\,\varphi_v^{(2)} = [\varepsilon_v^{(2)} - \Sigma^{(2)}(\varepsilon_v)]\,u_v . \tag{6}$$

The condition for solvability of this equation leads to the expression for the second-order correlation energy:

$$\varepsilon_v^{(2)} = \Sigma_{vv}^{(2)} .$$

It is a numerically demanding, but straight-forward, task to evaluate this correction. In Table 3, we show how the 10% errors found for the HF valence energies in cesium are reduced to the 1% level, after the second-order correlation corrections are added.

A formal solution to Eq.(\ref{aqpe}) is given by:

$$|\, v^{(2)} \,\rangle = \sum_{i \neq v} \frac{\Sigma_{iv}^{(2)}(\varepsilon_v)|\, i \,\rangle}{\varepsilon_v - \varepsilon_i} .$$

Substituting this into the Eq. 3, we may write the expression for the Brueckner-orbital transition matrix Z_{wv}^{BO} in the simple and elegant form:

$$Z_{wv}^{\mathrm{BO}} = \langle w|z|v^{(2)}\rangle + \langle w^{(2)}|z|v\rangle .$$

As we will show in later examples, the third-order BO corrections are the dominant correlation corrections to transition amplitudes.

The third-order structural-radiation corrections Z_{wv}^{SR} consist of thirty-

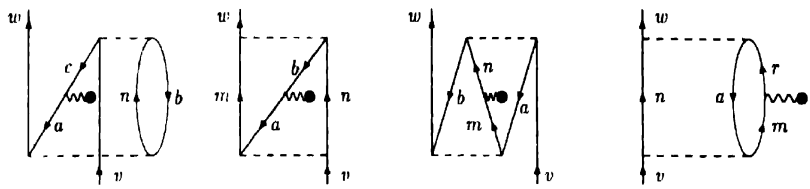

Fig. 6. Four of the thirty-six third order structural-radiation corrections.

six terms that are written out in detail in Ref. [10]. Four of these terms are given by the diagrams of Fig. 6. Finally, third-order normalization corrections are given by the expression [10]:

$$Z_{wv}^{\mathrm{Norm}} = -\frac{1}{2} Z_{wv}^{(1)} \left\{ \sum_{abm} \frac{v_{vmab} \tilde{v}_{abvm}}{(\varepsilon_v + \varepsilon_m - \varepsilon_a - \varepsilon_b)^2} + \sum_{amn} \frac{v_{vanm} \tilde{v}_{nmva}}{(\varepsilon_m + \varepsilon_n - \varepsilon_a - \varepsilon_v)^2} \right. \quad (7)$$

$$\left. + \sum_{abm} \frac{\tilde{v}_{wmab} v_{abwm}}{(\varepsilon_w + \varepsilon_m - \varepsilon_a - \varepsilon_b)^2} + \sum_{amn} \frac{\tilde{v}_{wanm} v_{nmwa}}{(\varepsilon_m + \varepsilon_n - \varepsilon_a - \varepsilon_w)^2} \right\}.$$

This term includes contributions required to normalize the many-electron wave function and contributions from "folded" diagrams [1].

It is a straight-forward, but tedious, task to evaluate all of the third-order corrections for a large atom such as cesium. In Table 4, we give a detailed breakdown of all corrections through third order for the $6p \rightarrow 6s$ and $7s \rightarrow 6p$ transitions in cesium. We see from this example that the 15% differences found in lowest-order are reduced to about 3% after third-order corrections are included. It is apparent from the table that the third-order BO corrections are the dominant correlation corrections.

Let us now turn to the continuum case and examine the role of third-order BO corrections in the low-energy photoionization of cesium. It is first necessary to solve the quasiparticle equation (4) in the continuum. In this case the energy is fixed. The short-range part of the scattering phase shift for a partial wave with angular momentum quantum number κ is given by $\delta_\kappa = \delta_\kappa^{\mathrm{HF}} + \delta_\kappa^{(2)}$, where

$$\delta_k^{(2)} = -\pi \langle u_\kappa | \Sigma^{(2)}(\varepsilon) | u_\kappa \rangle \quad (8)$$

In this equation, u_κ is the HF continuum wave function for the state (ε, κ).

Table 4. Contributions to the E_1 transition amplitudes for cesium.

Term	$6p_{1/2} \rightarrow 6s$	$6p_{3/2} \rightarrow 6s$	$7s \rightarrow 6p_{1/2}$	$7s \rightarrow 6p_{3/2}$
Z(1)	5.2777	7.4265	4.4135	6.6716
Z(2)	-0.3344	-0.4528	0.0448	0.0510
RPA(3)	0.0760	0.1005	-0.0150	-0.0174
RPA(4)+	-0.0446	-0.0604	0.0070	0.0084
BO(s)	-0.6226	-0.9263	0.8236	1.1615
BO(p)	0.0410	0.0842	-0.9305	-1.2343
SR	0.0445	0.0593	-0.0120	-0.0153
Norm	-0.0508	-0.0694	-0.0198	-0.0281
Z(Tot)	4.3964	6.1616	4.3116	6.5974
Experiment	4.499(6)	6.332(7)		

The p-wave phase shifts obtained by adding second-order correlation corrections to the HF phase shifts are shown in Fig. 7. It can be seen from this figure that the discrepancies with quantum defect theory found in the threshold HF phase shifts are almost completely removed once second-order Brueckner corrections are included.

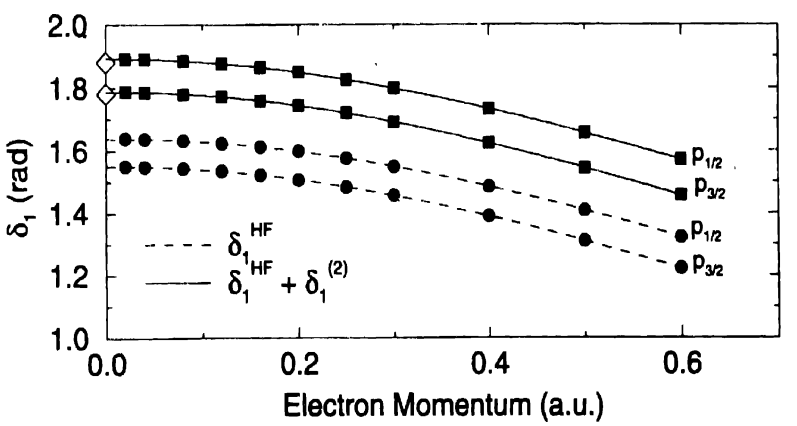

Fig. 7. Correlation corrections to p-wave electron-Cs^+ scattering phase shifts. The dashed lines give HF predictions, and the solid lines include second-order correlation corrections. The symbol ◊ represents phase shifts inferred from experiment using quantum defect theory.

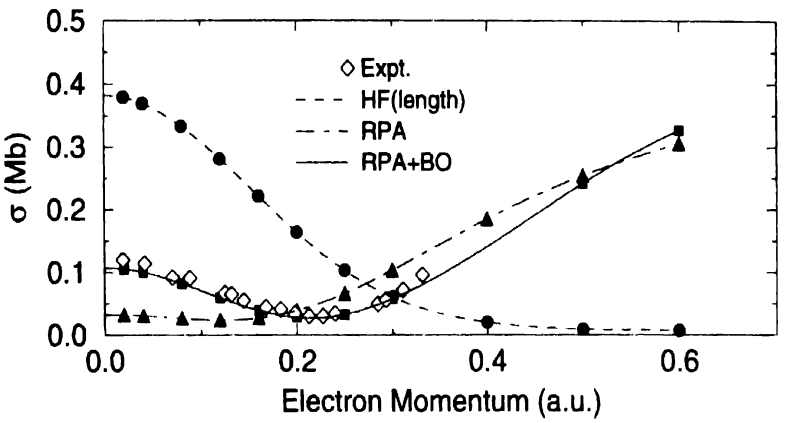

Fig. 8. Many-body calculations of the cesium photoionization cross section. HF, RPA, and the sum of RPA and third-order BO cross sections are presented. The ◊ symbol gives experimental values [9].

We may use the second-order Brueckner orbitals to evaluate the dominant third-order correlation corrections to the continuum p-wave transition amplitudes. The low-energy photoionization cross section for cesium obtained by including RPA and BO corrections in the amplitudes is shown in Fig. 8. We see that including both RPA and third-order BO corrections leads to theoretical cross section in good agreement with the measured cross section.

A more sensitive test of the continuum many-body calculations is the evaluation of the electron spin-polarization of cesium. This quantity, which gives the fraction of the photoelectrons that are spin-polarized in the direction of the incident photon beam for radiation that is 100% left-circular polarized, involves a delicate cancellation between $6s \to \varepsilon p_{1/2}$ and $6s \to \varepsilon p_{3/2}$ amplitudes. In Fig. 9, we compare the theoretical spin-polarization for cesium, given as a function of photon wavelength, with precise measurements [11,12]. The third-order calculations are seen to be in good agreement with the experimental values.

4.1 Electron-Xenon Elastic Scattering

When considering electron scattering from a neutral atom such as xenon, the electron-atom potential vanishes asymptotically faster than $-1/r$, in contrast to the case of cesium, where the potential at large distances is the ionic Coulomb potential. For scattering from an asymptotically neutral field, phase shifts take on limiting values governed by Levinson's theorem: the

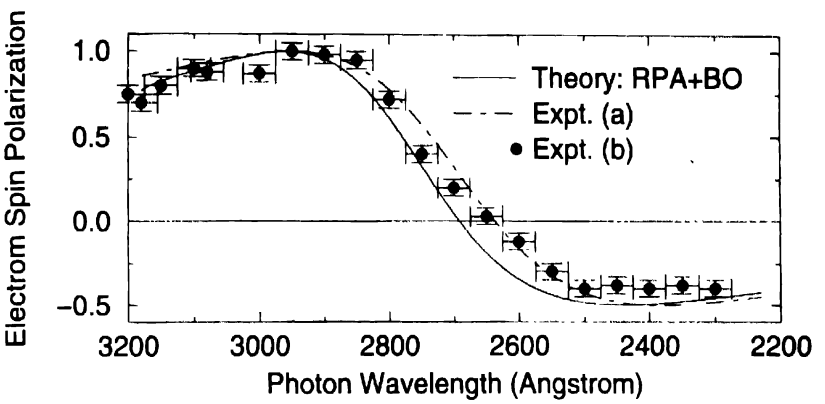

Fig. 9 Many-body calculations of the photoelectron spin-polarization given as a function of photon wavelength (Å) are compared with experimental values: (a) from Ref. [11], and (b) from Ref. [12].

zero-momentum phase shifts for angular momentum κ are related to N_κ, the number of occupied bound states with angular momentum κ, by $\delta_\kappa(0) = \pi N_\kappa$. Both HF phase shifts and correlated phase shifts in xenon satisfy this relation. We may obtain correlated scattering phase shifts for an electron moving in the field of a xenon atom by adding the second-order corrections given by Eq. (7) to the HF phase shifts. The phase shifts for *s*-waves, *p*-waves, ..., *h*-waves, found in this way, are plotted in Fig. 11. The dashed lines in the figure give the HF phase shifts and the solid lines give phase shifts that include second-order core-polarization corrections [13].

The *s*-wave phase shifts in the HF approximation, which govern the cross section near zero momentum, are seen to decrease in a monotone way from the threshold value $\delta_s(0) = 5\pi$. The corresponding HF scattering cross section, shown by the dashed line in Fig. 11, increases in a monotone way from threshold. This monotone behavior of the predicted HF cross section near threshold is in qualitative, as well as quantitative, conflict with experimental observations which show a pronounced minimum in the cross section just above threshold. This minimum in the low-energy scattering cross section is characteristic of elastic electron scattering from noble gas atoms; it is the well-known Ramsauer-Townsend minimum [14,15]. The Ramsauer-Townsend minimum was already understood to be a result of core polarization more than sixty years ago [16,17]. An analysis of the minimum similar to the present one was given for the case of argon in Ref. [18] and for helium, argon and xenon in Refs. [19,20].

In the upper left panel of Fig. 10, the *correlated* *s*-wave phase shift is

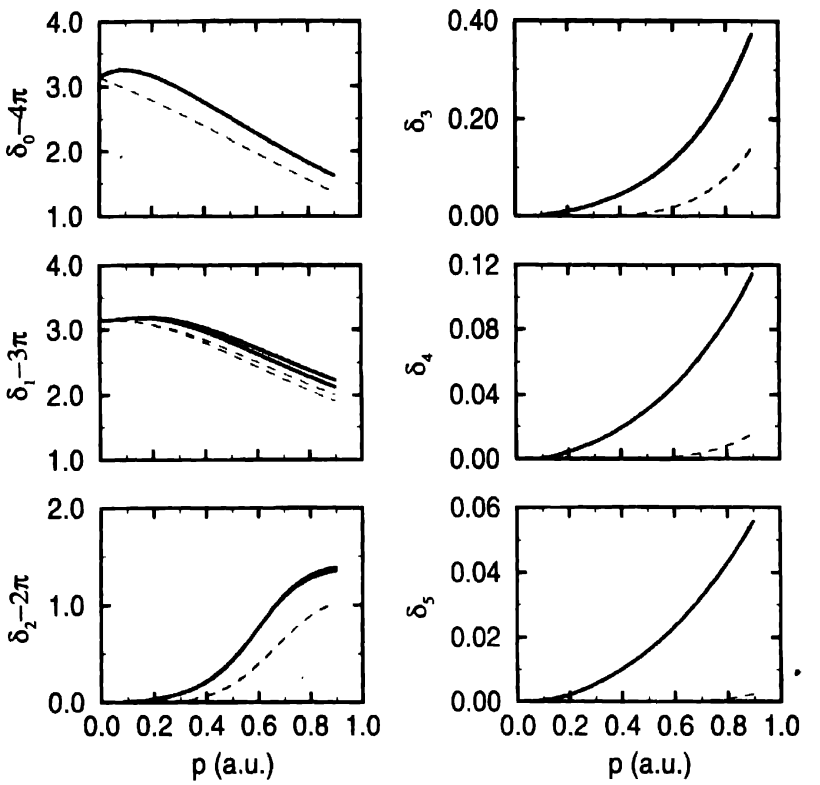

Fig. 10. Many-body calculations of the electron-xenon scattering phase shifts. Dashed lines represent HF approximation and solid lines give the correlation correction. Whenever distinguishable, the upper curve corresponds to the positive value of.the relativistic angular momentum κ and the lower curve to $\kappa < 0$.

shown to increase from 5π at threshold to a maximum at $p = 0.12$ a.u., and then to pass through 5π again at about $p = 0.23$ a.u., leading to a minimum in the cross section at the corresponding energy ≈ 0.7 eV. The corrections to s-wave and p-wave phase shifts are seen to be relatively small, ≈ 0.2 - 0.4 radian. For the d-waves and higher partial waves, on the other hand, the phase shifts at low energies are dominated by the correlation corrections! This is a consequence of the relatively long range of the electron self-energy operator, $\approx -\alpha_d/2r^2$,

In Fig. 11, we show both the HF and correlated predictions of the cross section as functions of energy. The essential role of correlation in the low-energy cross section is evident from this figure. The HF calculation seriously

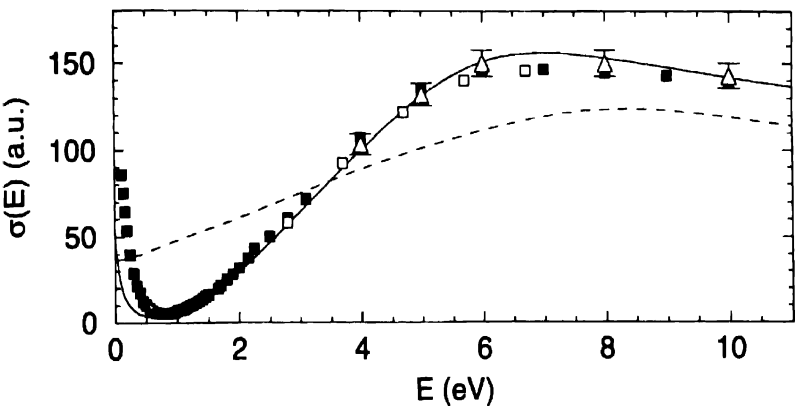

Fig. 11. Many-body calculations of the electron-xenon scattering elastic-scattering cross section. Dashed lines represent HF approximation and solid lines give the correlation correction. Experimental values: full squares, [21]; open squares, [22]; and open triangles, [23].

overestimates the cross section below 3 eV, and seriously underestimates it above 5 eV. The cross section is also compared with various experimental measurements [21,22,23] in the figure.

In summary, we have shown that photoexcitation and photoionization in heavy alkali-metal atoms, such as cesium, are described in a qualitatively correct way in the HF approximation. However, to obtain a quantitative understanding, it is found necessary to go beyond the central-field approximation and include both second-order core shielding and third-order core-polarization corrections. For elastic electron-xenon scattering, we have shown that the HF approximation fails to give even a qualitative understanding of the Ramsauer-Townsend minimum in the low-energy cross section. Going beyond the HF approximation and including core-polarization corrections to the phase shifts, however, leads to excellent quantitative agreement with the observed elastic scattering cross section.

References

[1] I. Lindgren and J. Morrison, *Atomic Many-Body Theory* (Springer, New York, 1991).

[2] P. O. Lowdin, J. Math. Phys. **3**, 1171 (1958).

[3] A. L. Fetter and J. D. Walecka, *Quantum Theory of Many-Particle Systems* (McGraw-Hill, New York, 1971).

[4] A. B. Migdal, *Theory of Finite Fermi Systems and Applications to*

Atomic Nuclei (Interscience, New York, 1967).

[5] V. A. Dzuba, V. V. Flambaum, P. G. Silvestrov and O. P. Sushkov, Phys. Lett. B **20**, 1399 (1987).

[6] C. E. Moore, *Atomic Energy Levels*, NSRDS-NBS 35 (U.S. GPO, Washington, 1971), vol. III.

[7] M. J. Seaton, Mon. Not. R. Astron. Soc. **118**, 504 (1958); U. Fano, Phys. Rev. A **2**, 353 (1970).

[8] C. Tanner, *Atomic Physics 14*, editors D. J. Wineland, C. E. Wieman and S. J. Smith (AIP Press, New York, 1995).

[9] H. Suemitsu and J. A. R. Samson, Phys. Rev. A **28**, 2752 (1983).

[10] S. A. Blundell, D. S. Guo, W. R. Johnson and J. Sapirstein, Atomic Data and Nuclear Data Tables **37**, 103 (1987).

[11] G. Baum, M. S. Lubell and W. Raith, Phys. Rev. Lett. **25**, 269 (1970).

[12] U. Heinzmann, J. Kessler and J. Lorenz, Z. Phys. **240**, 42 (1973).

[13] W. R. Johnson and C. Guet, Phys. Rev. A **49**, 1041 (1994).

[14] C. Ramsauer, Ann. Phys. (Leipz.) **64**, 513 (1921).

[15] J. S. Townsend and V. A. Bailey, Phil. Mag. **43**, 593 (1922).

[16] J. Holtzmark, Z. Phys. **55**, 437 (1929).

[17] N. F. Mott, Proc. Roy. Soc. A **124**, 425 (1929).

[18] Michael S. Pindzola and Hugh P. Kelly, Phys. Rev. A **9**, 323 (1974).

[19] M. Ya. Amusia, N. A. Cherepkov, L. V. Chernysheva and S. G. Shapiro, Phys. Lett. **46A**, 387 (1974).

[20] M. Ya. Amusia, N. A. Cherepkov, S. G. Shapiro and A. Tančić, Soviet Phys-JETP **68**, 2023 (1975).

[21] J. Ferch, F. Simon and G. Strakeljahn, in abstracts for *15th International Conference on Physics of Electronic and Atomic Collisions* (Brighton, 1987) unpublished.

[22] M. S. Dababneh, W. E. Kauppila, J. P. Downing, F. Laperriere, V. Pol, J. H. Smart and T. S. Stein, Phys. Rev. A **22**, 1872 (1980).

[23] J. C. Nickel, K. Imre, D. K. Register and S. Trajmar, J. Phys. B **18**, 125 (1985).